SUPPORTING INFORMATION FOR

Solution-Phase Structural Characterization of Supramolecular Assemblies by High-Angle Molecular Diffraction

Jodi L. O'Donnell, Xiaobing Zuo[†], Andrew J. Goshe[†], Lev Sarkisov[‡], Randall Q. Snurr[‡], Joseph T. Hupp, David M. Tiede[†]*

Department of Chemistry, Northwestern University, Evanston, IL 60208

[‡]Department of Chemical and Biological Engineering,

Northwestern University, Evanston, IL 60208

[†]Chemistry Division, Argonne National Laboratory, Argonne, IL 60439

*Corresponding author: Tel. 630-252-3539, fax: 630-252-9289

Email: tiede@anl.gov

Experimental Methods

Synthesis of molecular squares.

Assemblies 1 - 4 were synthesized as described previously, Scheme 2.[1,2] Briefly, equimolar quantities of $Re(CO)_5Cl$ and the desired difunctional ligand (see Scheme 2) were combined under nitrogen in 3:1 THF-toluene. The reaction mixture was heated at 60º for 48 hours. The precipitate was collected by filtration, rinsed with hexanes, and dried *in vacuo*. The 4,4'-bipyridine bridged square was further purified by recrystallization from hot acetone.

X-ray scattering analysis.

X-ray scattering data were collected at Sector 12 of the Advanced Photon Source[3] using 20 keV (0.62 Å) X-ray radiation, a Mar CCD area detector, and data acquisition procedures as described previously.[4-7] Scattering patterns were measured across the range of momentum transfer 0.04 $Å^{-1} < q < 6.8\ Å^{-1}$, where the scattering vector q equals $(4\pi/\lambda)\sin\theta$ and 2θ is the scattering angle. This required combining two sets of scattering data collected with sample-to-detector positions of 30 cm and 10 cm using a 2 mm diameter quartz capillary liquid flow cell and a 0.1 mm focused X-ray beam. Five sets of two-dimensional scattering patterns were collected using image integration times between 1 and 10 seconds. The absence of sample radiation damage was indicated by equivalence of scattering patterns measured for different integration times and with samples measured under high flow rates (<1 sec residence time in X-ray beam).

Two-dimensional scattering data of supramolecular square and background solvent samples were azimuthally averaged about the incident X-ray beam position, corrected for angle and pathlength dependent variations in X-ray absorption,[8] polarization, incoherent, and multiple

scattering[9] and calibrated for the scattering vector q. Final one-dimensional scattering patterns of scattered intensity versus q for the molecular squares were obtained by subtraction of the azimuthally averaged, intensity corrected and calibrated two-dimensional solution and solvent background data as described previously. [5-7]

X-ray scattering patterns for coordinate-based model structures used computational procedures described previously.[5-7,10] Atomic pair distribution functions (PDF), *P(r)*, for model structures were determined directly from coordinates as well as from the program GNOM that calculates PDF from scattering patterns using indirect Fourier transform methods.[11,12] The reproduction of equivalent PDF either calculated directly from coordinates or obtained from GNOM fits to calculated ideal scattering data demonstrated validity of these indirect methods for recovery of real-space distance correlations for these molecular structures. Both model and experimental PDF were determined using data truncated to the experimental range of momentum transfer 0.04 $Å^{-1} < q < 6.8\ Å^{-1}$ in order to ensure comparisons at the same spatial resolution and with the same truncation artifacts.

Solution phase molecular scattering patterns are produced by volume fraction and x-ray absorption weighted solvent background scattering subtraction from solution (solvent plus solute) scattering patterns.[4-7] The resulting difference reflects the small excess scattering due to the presence of the solute. An example of radially averaged scattering patterns for a 1 mM solution of compound 2 in dimethylformamide is shown in Figure S1, part A, compared with the background scattering for dimethylformamide alone. The solution scattering pattern can be seen to be dominated by scattering from the solvent. The difference pattern, Figure S1, Part B, shows scattering for compound 2 that can be distinguished from the solvent scattering. The main factor contributing to variation and uncertainty in measurement of the macromolecular solute

difference scattering pattern comes from uncertainty in determining the volume fraction and absorption corrections for the solvent background subtraction. In practice we find that small adjustments (< 1%) to the normalization constant for background subtraction must sometimes be applied to achieve a slope in the high *q* region to approximate slopes in model calculations. The broadness of the solvent diffraction peak compared with those of the molecular squares (Fig. S1) was found to make measurement of the molecular square solution diffraction peak positions and linewidths insensitive to uncertainties in the accuracy of solvent background subtraction.

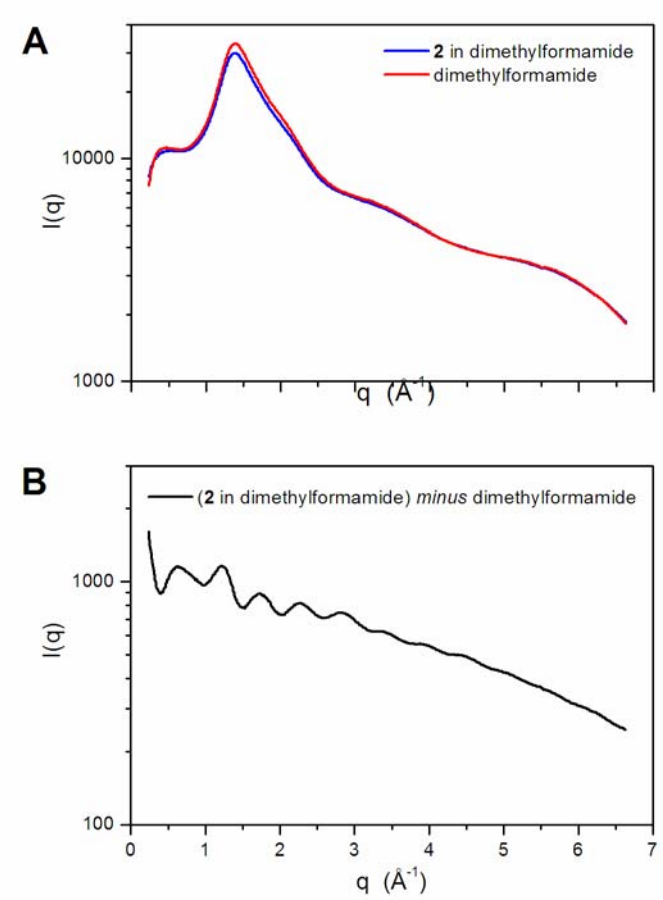

Figure S1. Experimental scattering patterns for 2. Panel A shows radially averaged scattering patterns measured for the solution (1 mM 2 in dimethylformamide) and the solvent alone for the range of momentum transfer 0.2 Å-1 < q < 6.8 Å-1. Panel B shows the uncorrected partial scattering pattern for this q range measured for 2 by subtraction of the solution and solvent scattering patterns.

Following background subtraction, a series of corrections were applied to the experimental scattering patterns as described below.

Data processing.

Scattering data require corrections for the pixel position dependent solid angle effect, angle and pathlength dependent X-ray absorption, polarization, incoherent, and multiple scattering.[8,9,13,14]. These corrections are illustrated in figure S2. First, X-ray scattering intensity at each pixel was corrected by multiplying a factor of $\cos^{-3}(2\theta)$, which compensates the pixel position dependent solid angle effect at Mar CCD detector imaging plate and applied to the radially averaged scattering pattern (Figure S2 red line). Pathlength dependent X-ray absorption profiles by the solvent for cylindrical capillary cell were numerically calculated. The absorption profile of scattered X-ray with energy of 20 keV was found to be negligible up to q = 7 $Å^{-1}$ and, therefore, no absorption correction were applied to the 20 keV scattered photons. However, the signal registered on the detector includes X-ray fluorescence photons, which emit at a lower energy (ca. 8.65 keV for Rhenium complex) and have a fairly strong q-dependent absorption profile. The absorption profile for Rhenium fluorescence at 8.65 keV was found to follow a polynomial decay fashion along q. A simulated angle-dependent fluorescence curve was then subtracted from the data to produce the green line in Figure S2. Finally solvent incoherent (or Compton) scattering was also considered in the experimental data corrections. The incoherent data for each element were taken from ref [15]. The amounts of Rhenium X-ray fluorescence and incoherent scattering were manually adjusted to make the corrected experimental data fall at a similar slope as that of calculated scattering patterns in the range of q > 1.0 $Å^{-1}$, with resulting

curve shown by the blue trace in Figure S2. Comparisons between experimental and model calculated scattering patterns are discussed in the text.

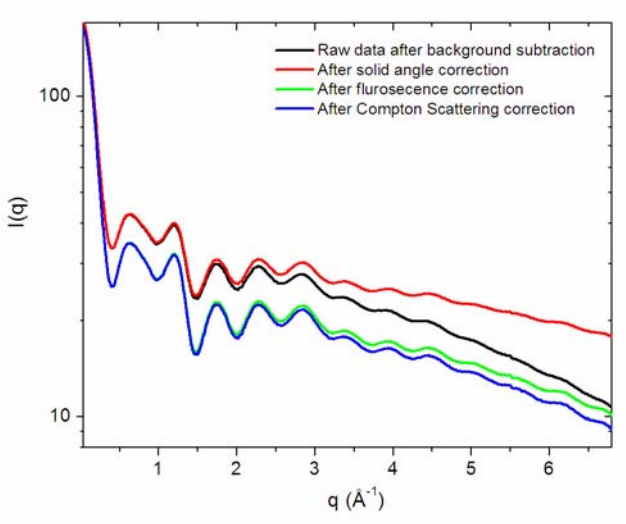

Figure S2. Empirical wide-angle X-ray scattering data corrections for Re-bipyridyl square **2**. The fluorescence and incoherent scattering values at q = 0 in this figure are 8.00 and 1.25, respectively.

Bipyridine molecular square structural models.

Detailed analysis of the conformational behavior of molecular squares 1 and 2 and their constituent building blocks was introduced previously.[16] Following the original approach, the Dreiding force field[17] was employed to model the bond stretching, bending, and torsional interactions within the bipyridine molecule. The non-bonded interactions were described using a Buckingham potential also with parameters taken from the Dreiding force field. No optimization of the potential parameters was performed. Since rhenium was not included in the original force field, the Re-N, Re-CO, and Re-Cl equilibrium distances were taken from the relevant crystal structures.

Lowest potential energy conformations were generated using the annealing approach commonly employed in molecular structure optimization.[18] Specific details of the protocol are described elsewhere.[16] Several variations of the original force field were tested. These variations

included rigid restrictions on the ligand structure around the rhenium corner post to keep this fragment in the crystal formation. We also considered intramolecular Coulombic interactions using Mulliken partial charges on the atoms generated from quantum mechanical density functional calculations at the B3LYP/LANL2DZ level.[19,20] The density functional calculations were performed using the Gaussian03 program.[21] These studies showed that the lowest energy conformation of the bypiridine molecular square is fairly insensitive to the introduced modifications of the force field.

The experimentally observed scattering patterns correspond to the conformational behavior of molecular squares averaged over a Boltzmann-weighted distribution of conformers. To explore this distribution we applied molecular dynamic simulation analysis, Figure S3. The simulations were carried out using Hyperchem 6.02 software with MM3 force field parameters at 300 K for 50 ps.[22] Energy minimizations and MD simulations were performed for a single square in vacuum, neglecting any solvent effects.

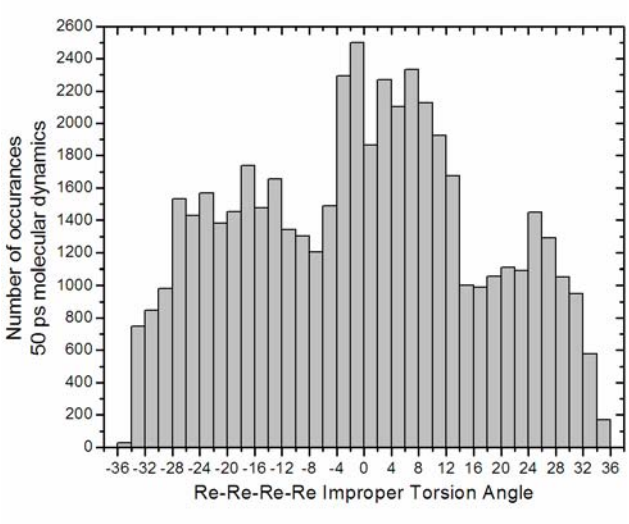

Figure S3. Rhenium improper torsion angles obtained from a 50 ps molecular dynamics simulation. Note that the distribution was approximately symmetric about zero and that the negative angles are identical to the positive by molecular inversion symmetry.

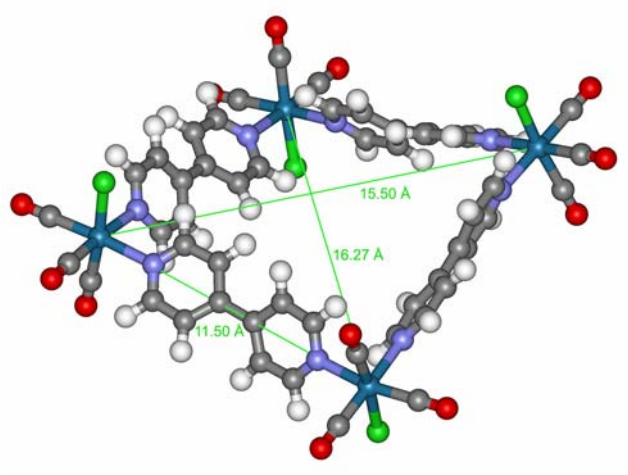

Figure S4. An alternate model with a reduced 2-fold symmetry element rather than the 4-fold symmetry seen in crystal structures and other models. The reduction in symmetry leads to an asymmetric puckering in which the side length remains the same as dictated by th eligand's presence, but the two diagonal distances are different from one another (Side 11.50Å; long diagonal: 16.27 Å; short diagonal 15.50 Å.) Essentially, in the above structure, one diagonal (short) is puckereed while the (long) other one is still relaxed. The Re-Re-Re-Re improper torsion angle is 24.1°, which corresponds to the one of the maxima observed in MD simulations, Figure S3. Side ligands were optimized in Spartan04 (MM) while all Re atoms were fixed.

References:

(1) Slone, R. V.; Hupp, J. T.; Stern, C. L.; Schmitt, T. E. A. *Inorg. Chem.* **1996**, *35*, 4096.
(2) Graves, C. R.; Merlau, M. L.; Morris, G. A.; Sun, S.-S.; Nguyen, S. T.; Hupp, J. T. *Inorg. Chem.* **2004**, *43*, 2013-2017.
(3) Seifert, S.; Winans, R. E.; Tiede, D. M.; Thiyagarajan, P. *J. Appl. Crystallogr.* **2000**, *33*, 782-784.
(4) Tiede, D. M.; Zhang, R.; Seifert, S. *Biochemistry* **2002**, *41*, 6605-6614.
(5) Tiede, D. M.; Zhang, R.; Chen, L. X.; Yu, L.; Lindsey, J. S. *J. Am. Chem. Soc.* **2004**, *126*, 14054-14062.
(6) Zuo, X.; Tiede, D. M. *J. Am. Chem. Soc* **2005**, *127*, 16-17.
(7) Zuo, X.; Cui, G.; Mertz, K. M.; Zhang, L.; Lewis, F. D.; Tiede, D. M. *Proc. Natl. Acad. Sci. U.S.A.* **2006**, *103*, 3534-3539.
(8) Paalman, H. H.; Pings, C. J. *J. Appl. Phys.* **1962**, *33*, 2635-2639.
(9) Warren, B. E. *X-Ray Diffraction*; Dover Publications: New York, 1990.
(10) Zhang, R.; Thiyagarajan, P.; Tiede, D. M. *J. Appl. Crystallogr.* **2000**, *33*, 565-568.
(11) Svergun, D. I.; Semenyuk, A. V.; Feigin, L. A. *Acta Crystallogr., Sect. A: Found. Crystallogr.* **1988**, *44*.
(12) Svergun, D. I. *J. Appl. Crystallogr.* **1992**, *25*, 495-503.
(13) Jeong, I.-K.; Thompson, J.; Proffen, T.; Perez, A.; Billinge, S. J. L. *J. Appl. Cryst.* **2001**, *34*, 536-.
(14) Barna, S. L.; Tate, M. W.; Grunner, S. M.; Eikenberry, E. F. *Rev. Sci. Instr.* **1999**, *70*, 2927-2934.
(15) Wilson, A. J. C. In *International Tables for Crystallography*; Prince, E., Ed.; Springer, 1999; Vol. C.
(16) Miljacic, L.; Sarkisov, L.; Ellis, D. E.; Snurr, R. Q. *J. Chem. Phys.* **2004**, *121*, 7228-7236.
(17) Mayo, S. L.; Olafson, B. D.; Goddard, W. A. *J. Phys. Chem.* **1990**, *94*, 8897-8909.
(18) Leach, A. R. *Molecular Modelling Principles and Applications*; Addison Wesley Longman: Harlow, Essex, U.K., 1996.
(19) Becke, A. D. *J. Chem. Phys.* **1993**, *98*, 5648-5652.
(20) Hay, P. J.; Wadt, W. R. *J. Chem. Phys.* **1985**, *82*, 270-283.
(21) Frisch, M. J. T., G. W.; Schlegel, H. B.; Scuseria, G. E.; Robb, M. A.; Cheeseman, J. R.; Zakrzewski, V. G.; Montgomery, J. A., Jr.; Stratmann, R. E.; Burant, J. C.; Dapprich, S.; Millam, J. M.; Daniels, A. D.; Kudin, K. N.; Strain, M. C.; Farkas, O.; Tomasi, J.; Barone, V.; Cossi, M.; Cammi, R.; Mennucci, B.; Pomelli, C.; Adamo, C.; Clifford, S.; Ochterski, J.; Petersson, G. A.; Ayala, P. Y.; Cui, Q.; Morokuma, K.; Malick, D. K.; Rabuck, A. D.; Raghavachari, K.; Foresman, J. B.; Cioslowski, J.; Ortiz, J. V.; Baboul, A. G.; Stefanov, B. B.; Liu, G.; Liashenko, A.; Piskorz, P.; Komaromi, I.; Gomperts, R.; Martin, R. L.; Fox, D. J.; Keith, T.; Al-Laham, M. A.; Peng, C. Y.; Nanayakkara, A.; Gonzalez, C.; Challacombe, M.; Gill, P. M. W.; Johnson, B.; Chen, W.; Wong, M. W.; Andres, J. L.; Gonzalez, C.; Head-Gordon, M.; Replogle, E. S.; Pople, J. A., *Gaussian 98,* Revision A.7; Gaussian Inc.: Pittsburgh, PA, 1998.
(22) *HyperChem 6.02*; HyperCube, Inc.: Gainsville, FL, 2003.